J Therm Anal Calorim (2011) 106:7–24
DOI 10.1007/s10973-011-1496-7

The rigid amorphous fraction in semicrystalline macromolecules

Joseph D. Menczel

NATAS2010 Conference Special Issue

Abstract The first experimental evidence of the existence of the rigid amorphous fraction (RAF) was reported by Menczel and Wunderlich for several semicrystalline polymers. It was observed that the hysteresis peak at the glass transition was absent when these polymers were heated much faster than they had previously been cooled. In the glass transition behavior of poly(ethylene terephthalate) (PET), the hysteresis peak gradually disappeared as the crystallinity increased. At the same time, it was noted that the ΔC_p of higher crystallinity PET samples was much smaller than could be expected on the basis of the crystallinity calculated from the heat of fusion. It was also observed that this behavior was not unique to PET only, but is characteristic of most semicrystalline polymers: the sum of the crystallinity calculated from the heat of fusion and the amorphous content calculated from the ΔC_p at the glass transition is much less than 100% (a typical difference is $\sim$20–30%). This 20–30% difference was attributed to the existence of the "RAF". The presence of the RAF also affected the unfreezing behavior of the "mobile (or traditional) amorphous fraction." As a consequence, the phenomenon of the enthalpy relaxation diminished with increasing rigid amorphous content. It was suggested that the disappearance of the enthalpy relaxation was caused by the disappearance or drastic decrease of the time dependence of the glass transition. To check the validity of this suggestion, the glass transition had to be also measured on cooling in order to overlay it on the DSC curves measured on heating. However, before this overlaying work could be accomplished, the exact temperatures on cooling had to be determined since the temperature of the DSC instruments that time could not be calibrated on cooling using the usual low molecular weight standards due to the common phenomenon of supercooling. Therefore, a temperature calibration method needed to be developed for cooling DSC experiments utilizing high purity liquid crystals using the isotropic → nematic, the isotropic → cholesteric, and other liquid crystal → liquid crystal transitions. After the cooling calibration was accomplished, the cooling glass transition experiments indicated that the glass transition in semicrystalline polymers is not completely time independent, because its width depends on the ramp rate. However, it was shown that the time dependence is drastically reduced, and the midpoint of the glass transition seems to be constant which can explain the absence of the enthalpy relaxation. The work presented here has led to a number of studies showing the universality of the rigid amorphous phase for semicrystalline polymers as well as an ASTM standard for DSC cooling calibration.

Keywords DSC · Semicrystalline polymers · Rigid amorphous fraction · Temperature calibration of DSC's on cooling · Enthalpy relaxation · Time dependence of the glass transition

List of symbols

α	Fractional crystallinity
β	Amorphous content
Ch	Cholesteric phase
$C_m(T)$	Specific heat capacity of the amorphous phase

A shortened version of the Mettler-Toledo Award lecture at the 38th Annual NATAS Meeting, August 15–18, 2010, Philadelphia, PA.

Joseph D. Menczel—Retired.

J. D. Menczel (✉)
Alcon Laboratories (retired), 412 Stampede Court, Fort Worth, TX 76123, USA
e-mail: jmenczel@yahoo.com

$C_x(T)$	Specific heat capacity of the crystalline phase
C_p	Specific heat capacity
CR	Cooling rate
ΔC_p	Heat capacity jump at the glass transition
$H_{0\rightarrow T}$	Absolute enthalpy at a temperature T
HR	Heating rate
I	Isotropic phase
LC	Liquid crystal or liquid crystalline
N	Nematic phase
S	Smectic phase
$T_{clearing}$	Clearing point (nematic- or cholesteric-to-isotropic transition temperature)
T_{co}	Starting temperature of crystallization during cooling
T_g	Glass transition temperature
T_{itn}	Isotropic-to-nematic transition temperature
T_m	Melting point
T_m°	Equilibrium melting point
T_{real}	Real temperature in a DSC scan
T_{ind}	Indicated temperature in a cooling DSC scan
T_t	Transition temperature in a liquid crystal
$T_{unfreeze}$	End-temperature of unfreezing of the rigid amorphous fraction
$\Delta T = T_{real} - T_{ind}$	The difference between the real and indicated temperature in a cooling run

Abbreviations

BCH52	Liquid crystal 4′-ethyl-4-(4-propyl-cyclohexyl)-biphenyl
CE-3	Liquid crystal (+)-4-*n*-hexyloxyphenyl-4′-(2″-methylbutyl)-biphenyl-4-carboxylate
CE-8	Liquid crystal (+)-(4-(2′-methylbutyl)phenyl-4′-*n*-octylbiphenyl-4-carboxylate)
Ch	Cholesteric phase
HP53	Liquid crystal [4-(4-pentyl-cyclohexyl)-benzoic acid-4-propylphenyl ester
I	Isotropic phase
LC-1	Liquid crystal *N*-(4-*n*-octyloxy-2-hydroxybenzal)-4′-*n*-butylaniline
M24	Liquid crystal (4-cyano-4′-octyloxybiphenyl)
N	Nematic phase
RAF	Rigid amorphous fraction
TAF	Traditional (or mobile) amorphous fraction
PCL	Polycaprolactone
PBT	Poly(butylene terephthalate)
PEN	Poly(ethylene-2,6-naphthalene dicarboxylate), poly(ethylene naphthalate)
PET	Poly(ethylene terephthalate)
PP	Polypropylene
PPO	Poly(oxy-2,6-dimethyl-1,4-phenylene)
PVF	Poly(vinyl fluoride)

Introduction

The glass transition of amorphous polymers is a kinetic transition, thus it has considerable time dependence. One of the consequences of this time dependence is the appearance of the so-called hysteresis peak (enthalpy relaxation) when the sample is cooled much slower through the glass transition than it is reheated. Thus, it was a surprise when no enthalpy relaxation was observed for the first main chain liquid crystalline polymer [poly(ethylene terephthalate-co-p-oxybenzoate) with 60 and 80 mol% ethylene terephthalate units [1–3]. Since this specific glass transition involved the ethylene terephthalate-rich segments of the copolymer, we searched for the source of the absence of the hysteresis peak in the PET homopolymer. During this search, gradual disappearance of the hysteresis peak with increasing crystallinity of PET was confirmed. It was also noted that the higher crystallinity samples showed a much smaller ΔC_p than could be expected on the basis of the crystallinity calculated from the heat of fusion.

In the present work, the effect of the rigid amorphous fraction (RAF) on the traditional amorphous fraction (TAF) will be discussed: the hysteresis peak at the glass transition of the TAF disappears under the influence of the RAF, and this raises the question whether the glass transition of the TAF becomes time independent in semicrystalline polymers. It should be mentioned that here we talk about the hysteresis peak which is the consequence of slow cooling followed by fast reheating. However, an endothermic hysteresis peak on the high temperature side of the glass transition in semicrystalline polymers still can be introduced by annealing below the glass transition temperature. Nevertheless, an enthalpy relaxation caused by sub-T_g annealing is different from the one caused by slow cooling, because in the case of sub-T_g annealing the glass transition is preceded by an extremely broad exothermic hysteresis peak, so the reason for this phenomenon is not known so far.

Experimental

This work encompasses a considerable time frame, i.e., since 1980 till 2006. Thus, the DSC measurements were carried out on a number of different instruments. The measurements were started on a DuPont (today TA Instruments) DSC 910 connected to a DuPont 990 and 1090 Thermal Analyzers, and also on a Perkin-Elmer DSC4. Later, several Perkin-Elmer DSC7s, a TA Instruments 2100-910 DSC, a TA Instruments 3200-DSC 2920,

and a TA Instruments Q200 DSC were used. Most of these instruments (except the DSC 910-Thermal Analyzer 990 of DuPont) were cooled with some FTS mechanical cooling accessory having a head temperature of −100 °C. The instruments were calibrated with high purity water, In, Sn, and Pb on heating. When cooling calibration was necessary, this was done using (4-*n*-octyloxy-2-hydroxy-benzal)-4′-*n*-butylaniline (labeled as LC-1), (+)-(4-(2′-methylbutyl)phenyl-4′-*n*-octylbiphenyl-4-carboxylate (with a commercial name of CE-8®), and (+)-4-*n*-hexyloxyphenyl-4′-(2″-methylbutyl)-biphenyl-4-carboxylate having a commercial name of CE-3® [4–6]. CE-3 and CE-8 were purchased from BDH Chemicals Ltd., Poole, Gt. Britain [7] purified to ~99.9% as described in [4–6].

The following polymers were used in this series of studies: PET, Nylon 6, PVF, Nylon 66, polypropylene, poly(ethylene-2,6-naphthalene dicarboxylate) (PEN), and polycaprolactone (all from Scientific Polymer Products); fiber grade PET of Hoechst Celanese with IV of 0.65; Gafite 1600 PBT from GAF Corporation; Lexan polycarbonate from GE (crystalline polycarbonate was prepared from Lexan as described in [8]).

Results and discussion

Deficiency of ΔC_p at the glass transition

The two-phase model of semicrystalline polymers assumes that any semicrystalline polymer is composed of a crystalline fraction and an amorphous fraction. Thus,

$$C_p(T) = \alpha C_x(T) + \beta C_m(T) = \alpha C_x(T) + (1-\alpha)C_m(T), \quad (1)$$

where $C_p(T)$ is the temperature dependence of the specific heat capacity of the semicrystalline polymer, $C_x(T)$ is the temperature dependence of the specific heat capacity of the crystalline phase, $C_m(T)$ is the temperature dependence of the specific heat capacity of the amorphous phase, α is the fractional crystallinity calculated from the heat of fusion, and β is the amorphous fraction calculated from the heat capacity jump at the glass transition. Therefore, according to the two-phase model:

$$\beta = 1 - \alpha \quad (2)$$

DSC experiments carried out on PET and several other semicrystalline polymers [1] indicated that the sum of α calculated from the heat of fusion and β calculated from the ΔC_p does not add up to 100%. Therefore,

$$\beta \neq 1 - \alpha. \quad (3)$$

For most polymers studied, the value of $1 - \alpha - \beta$ was around 20–30%, and it was suggested that some "RAF" is responsible for the missing ΔC_p. In [1], it was proposed that "Most likely the cause of this different behavior is the crystal-amorphous interface, the structure of which is the object of much current debate." and "A more detailed discussion must await quantitative separation of the heat capacity contributions and a study of the morphology of the crystals. Both topics are under investigation in our laboratory." [1]. Thus,

$$\text{RAF} = 1 - \alpha - \beta. \quad (4)$$

As it was suggested in [1, 8], the RAF can be determined if the fraction of the traditional amorphous phase is determined from the heat capacity jump at the glass transition, and the crystallinity is calculated from the heat of fusion.

PET and PEN are two very convenient polymers for studying the RAF, because samples with vastly different crystallinities can be prepared by just changing the thermal history, i.e., the rate of cooling from the melt. Then if these samples are heated in the DSC, qualitatively the DSC curves look as expected, i.e., the heat capacity jump at the glass transition increases with increasing cooling rate (decreasing crystallinity). The heating DSC curves of samples of PET prepared by cooling at a rate of 2, 5, 10, and 20 °C/min are shown in Fig. 1. However, the absolute magnitude of the heat capacity increase at the glass transition is much less than should be on the basis of crystallinity calculated from the heat of fusion.

A full DSC curve for semicrystalline PET is shown in Fig. 2a. This was the first DSC curve in the literature showing the presence of the RAF [1]: the RAF was ca. 18% when calculated from the heat of fusion and the heat capacity increase at the glass transition. Similar results were obtained for poly(ethylene naphthalate) (PEN, see Fig. 2b). These experimental data indicate the presence of a transitional layer on the crystal surfaces, and also that the crystal surfaces are linked to the amorphous phase by tie

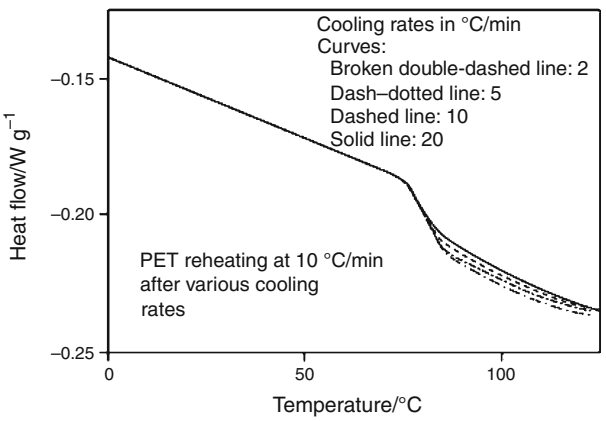

Fig. 1 Heating curves of PET samples in the glass transition region prepared by cooling from the melt at 2, 5, 10, and 20 °C/min. As can be seen, ΔC_p increases with increasing cooling rate. TAI Q200 DSC, endotherm is down

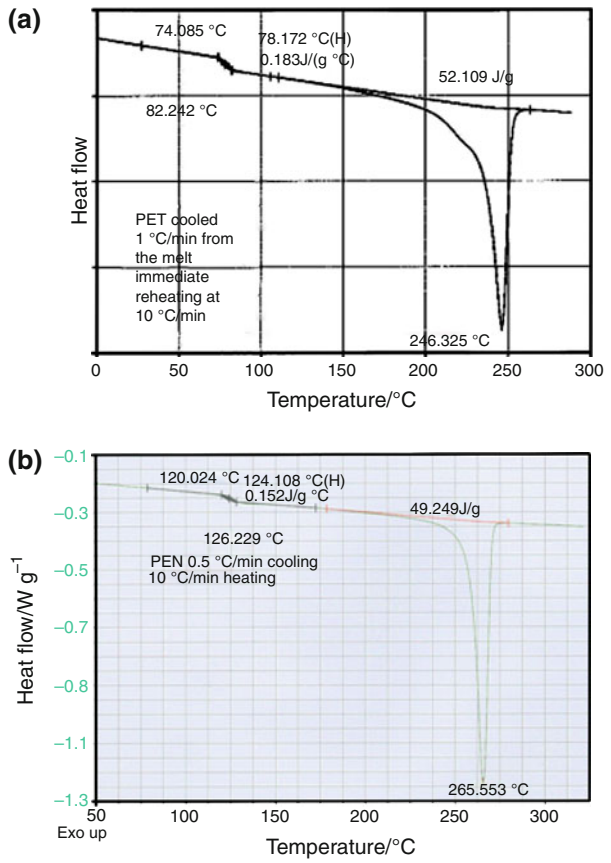

Fig. 2 (**a**) Heating curve of PET crystallized from the melt at a rate of cooling of 1 °C/min (heating rate = 10 °C/min). It is obvious that $\alpha + \beta < 1$, i.e., a considerable RAF is present in the sample (endo down) (TAI Q200 DSC) (ΔC_p for amorphous PET is 77.8 J/(°C mol), and the heat of fusion of 100% crystalline PET is 26.90 kJ/mol. (**b**) Heating curve of poly(ethylene naphthalate) (PEN) crystallized from the melt at a rate of cooling of 0.5 °C/min (heating rate = 10 °C/min) (ΔC_p for amorphous PEN is 80.1 J/(°C mol), and the heat of fusion of 100% crystalline PEN is 24.02 kJ/mol). Like for PET, $\alpha + \beta < 1$, i.e., a considerable RAF is present (endo down) (TAI Q200 DSC). Both samples, PET and PEN were heated beyond T_m°, held there for 2 min in order to destroy any ordered regions, cooled at 10 °C/min to ca. T_{co}+20 °C to minimize degradation, and finally, cooled at 1 and 0.5 °C/min to −80 °C in order to crystallize the samples and go much below T_g

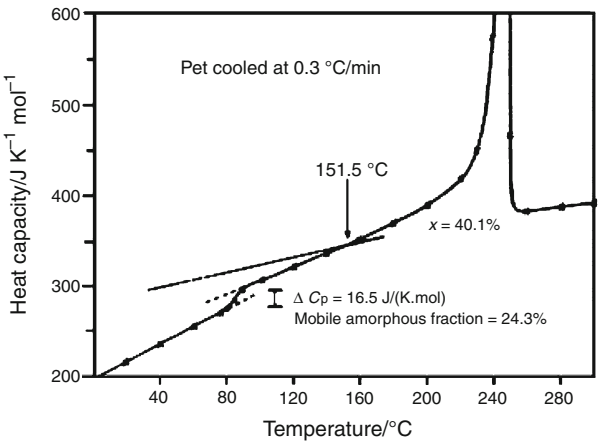

Fig. 3 Determination of the endpoint of unfreezing of the RAF by heat capacity measurements (from [8]). Measurements on a Perkin-Elmer DSC4. RAF = 40.1%, TAF = 24.3%. The straight line below 151.5 °C indicates the temperature dependence of the specific heat capacity of semicrystalline PET of the present crystallinity above the T_g of TAF that would have been obtained on the basis of the two-phase model. The *arrow* indicates the final temperature of unfreezing of the RAF

molecules. Thus, the crystals partially immobilize the amorphous phase. This linking and the surface layer are responsible for the broadening of the glass transition of the traditional amorphous phase, the appearance of the RAF, and also the disappearance of the hysteresis behavior at T_g. In most polymers, the RAF unfreezes at higher temperatures than the TAF. Wunderlich [9] lists several polymers in which the RAF unfreezes at T_g of the TAF. In the simplest case, when T_g of the RAF is between T_g of the TAF and start of the melting of the crystals, simple heat capacity measurements may determine the endpoint of unfreezing of the RAF (see, e.g., Fig. 3). However, the determination of the temperature range of unfreezing of the RAF is not always easy, because crystal reorganization may interfere above the T_g of the TAF.

When checking other semicrystalline polymers [Nylon 6, Nylon 66, poly(vinyl fluoride), polycaprolactone, bisphenol-A-polycarbonate, poly(butylene terephthalate)], the sum of the amorphous content calculated from the ΔC_p at the glass transition and the crystallinity calculated from the heat of fusion was far from 100% [1, 8]. Although the sample preparation conditions do have a considerable influence on the sum of the crystallinity and the TAF, this number for most polymers studied in [1, 8] was around 0.7, meaning that the RAF was ca. 30%. Thus, the presence of the RAF was confirmed in five semicrystalline polymers: PET, Nylon 6, PVF, Nylon 66, and polycaprolactone [1] (see Figs. 3, 4) and later for polyoxymethylene [10]. Somewhat later poly(butylene terephthalate) and bisphenol-A polycarbonate [8] were added to this list.

The temperature range of unfreezing of the RAF cannot be seen directly from the DSC curves as is the case of the TAF. It can be suggested that for most polymers, the unfreezing of the RAF starts as soon as the unfreezing of the TAF is over (except those cases listed by Wunderlich in [9] where the unfreezing may proceed at temperatures as high as the start of the melting). It is more difficult to determine the end-point of the unfreezing of the RAF, because often crystal reorganization can take place between the end-point of unfreezing of the TAF and the beginning of the melting process. Wunderlich gave a summary for this, including the various types of the RAF [9]. In the simplest case when between T_g and beginning of

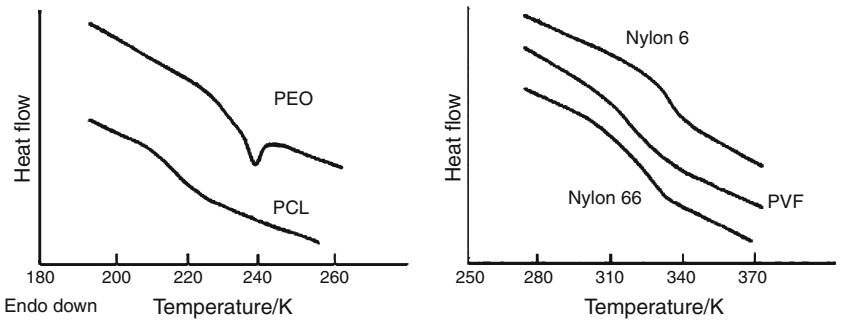

Fig. 4 The heating DSC curves of several high crystallinity semicrystalline polymers in the glass transition region prepared by slow cooling from the melt and reheated at 20 °C/min: Nylon 6 cooled at 0.5 °C/min from 300 °C; poly(vinyl fluoride) cooled at 0.5 °C/min from 230 °C; Nylon 66 cooled at 0.5 °C/min from 300 °C; poly(ethylene oxide) cooled at 2 °C/min from 120 °C; and polycaprolactone cooled at 2 °C/min from 80 °C. In addition to the missing hysteresis peak, ΔC_p at the glass transition is too small for the amorphous fraction as calculated from the crystallinity on the basis of the two-phase model (from [1]). Measurements on a DuPont 990-910 DSC. Figure reproduced from [1]

melting, only heat capacity increase takes place, the end-point of unfreezing of the RAF can be determined as shown in Fig. 3 for PET. Here, the straight line indicates the temperature dependence of the heat capacity of the polymer calculated on the basis of the two-phase model.

When this method is applied to samples of a polymer of different thermal histories, the unfreezing of the RAF may give some information about the structure of the RAF. Such a case is presented in Fig. 5 for PBT of different crystallinities. The numerical data are summarized in Table 1: it is clear that the end-point of unfreezing (T_{unfreeze}) of the RAF cannot be correlated with the amount of the RAF, but it is the function of the crystallinity. More work is necessary in this area, and this can be helpful in clarifying the structure of the RAF.

All this indicates that the structure of the amorphous phase is not that simple as was thought 30–40 years ago. Since then, a number of publications dealt with studying the structure of the RAF. An excellent summary paper is given by Wunderlich [9]. Modulated-temperature DSC [11–14], dielectric analysis [15, 16], and density measurements [17, 18] also became important in studying the structure of the RAF. Even techniques like TEM [19, 20], X-ray diffraction, and solid state NMR [21, 22] were applied.

Temperature calibration on cooling

In [1], normal hysteresis behavior was found for the glass transition of amorphous PET, i.e., an endothermic hysteresis peak appears at the high temperature side of the glass transition when the sample is heated faster than it had previously been cooled. As expected for amorphous polymers, the magnitude of the endothermic hysteresis peak increases with decreasing cooling rate (see Figs. 12, 13). However, when crystallinity is introduced into the sample, the intensity of the hysteresis peak gradually decreases (Fig. 17) and disappears at a crystallinity value of 29% as can be seen in Fig. 18 (in the original paper of [1], 30% was obtained). Therefore, in [1], it was suggested that the time dependence of the glass transition may disappear at high crystallinity values. To prove this, it would be useful to overlay the DSC curves recorded in a cooling experiment on the heating DSC curves of the glass transition, but in 1980 (when the original paper [1] on the RAF was published) the thermal analysis instrumentation was not sophisticated enough to accurately record the glass transition on cooling.

On the DuPont 910 DSC, the quench cooler (stainless steel cooling can) or cold purge gas was the only available cooling options. Therefore, the cooling baseline was not reproducible, so superposition of the cooling and heating curves was not possible and the time dependence of the glass transition could not be experimentally checked. Later with introduction of the FTS mechanical cooling accessories and modification of the sample holders for better cooling performances, this task became much easier especially with the DSC's of Tzero technology. When using mechanical cooling accessories, the temperature control is not lost during cooling at reasonable rates, and the baselines are well reproducible during cooling at various rates. There was another problem that needed to be solved in order to overlay the cooling and heating DSC curves on each other: the instruments before 1980 could be calibrated only on heating, because the melting point of high purity metal and organic substances were used for calibration, and it is well known that the freezing point is always lower than the melting point due to supercooling. Thus, a suitable thermal transition had to be found that occurs at the same temperature on heating as it does on cooling. Such transitions include certain magnetic

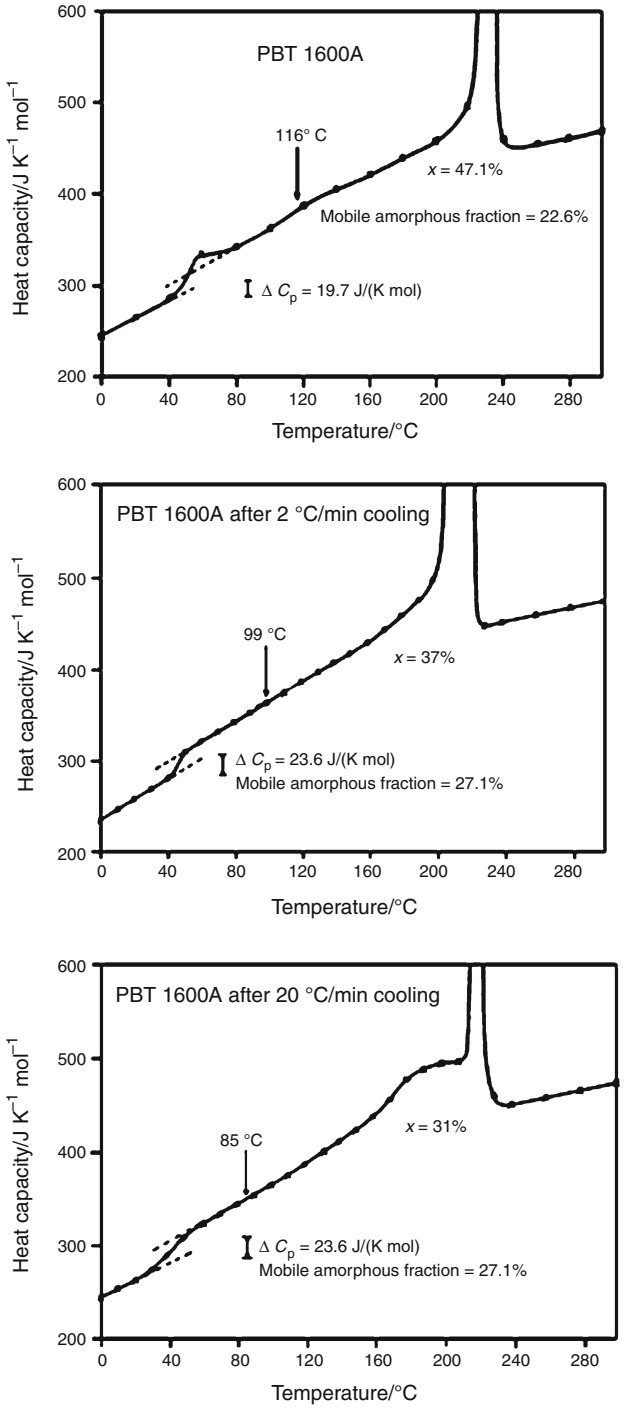

Fig. 5 Determination of the end-temperature of unfreezing of the RAF ($T_{unfreeze}$) for PBT samples of various crystallinities (compare with Fig. 3). *Top figure* As-received PBT (pelletized); *middle figure* PBT crystallized at a cooling rate of 2 °C/min; *bottom figure* PBT crystallized at a cooling rate of 20 °C/min. As can be seen, $T_{unfreeze}$ increases with increasing crystallinity and is not correlated with the content of the RAF

transitions, secondary transitions (but it is rather difficult to apply these in a DSC), and some first-order transitions involving liquid crystals, namely the nematic → isotropic

Table 1 The end-temperature of unfreezing of the RAF for poly(butylene terephthalate) samples of various crystallinities

Sample	Crystallinity	ΔC_p/ J mol^{-1} K^{-1}	TAF	RAF	$T_{unfreeze}$*
As-received (high pressure crystallization)	0.47	17.8	0.204	0.326	116
After 2 °C/min cooling	0.37	19.4	0.223	0.407	99
After 20 °C/min cooling	0.31	24.3	0.279	0.411	85

* $T_{unfreeze}$ can be correlated with crystallinity and not RAF. Similar results were obtained for PET

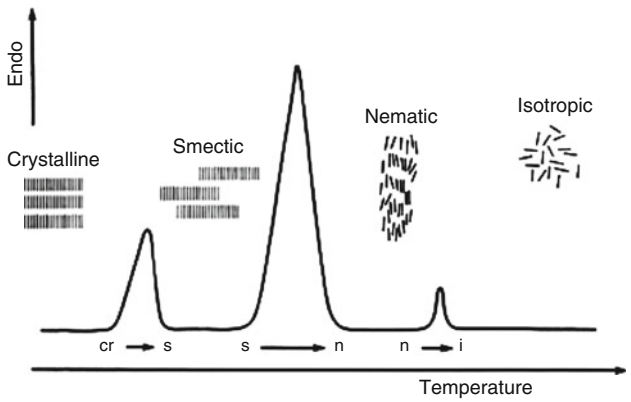

Fig. 6 A schematic DSC curve of a low molecular weight smectic liquid crystal. The peaks from *left to right*: crystal to smectic, smectic to nematic, and nematic to isotropic

and cholesteric → isotropic transitions. These latter ones do not have transition temperature hysteresis on cooling, because the nuclei of the nematic or cholesteric phase are always present in the isotropic melt due to density fluctuations. Menczel and Leslie [4–6] were the first to apply these transitions for temperature calibrations of DSC's on cooling.

The traditional small molecular mass liquid crystals consist of long, rodlike molecules (the molecules of the other type of liquid crystals, the so-called discotic ones, as their name implies, are composed of molecules of discotic shape). When the long axes of these molecules have a preferential direction, i.e., most of them are directed into one direction, called the optic axis (or director), the phase is called "nematic" (Fig. 6). The basic idea of the temperature calibration of DSC's on cooling is, as mentioned before, that the isotropic → nematic [or isotropic → cholesteric (also called twisted nematic)] transition occurs at the same temperature on cooling than it does on heating. Figure 7 shows a schematic of this transition. A small area is encircled in the left figure indicating a nematic nucleus

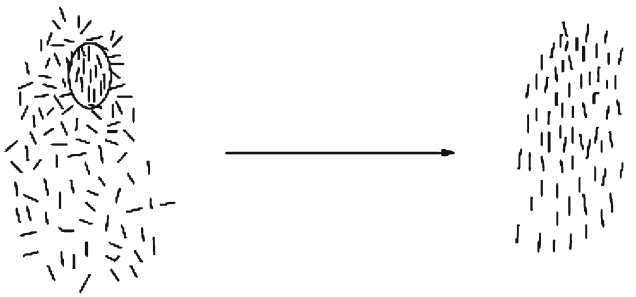

Fig. 7 A schematic representation of the isotropic → nematic transition for a liquid crystal consisting of rodlike molecules. The *encircled area* in the isotropic melt shows a nucleus of the nematic phase

in the isotropic liquid that was formed owing to density fluctuations. These nuclei are the ones responsible for initiating the transition during cooling at the same temperature as on heating.

The basic requirements for selecting a standard for cooling calibration of DSCs are the following:

(a) the selected transition must take place at the same temperature on heating as it does on cooling, i.e., the transition must not have a hysteresis;
(b) the selected transition must be narrow, i.e., the transition must be a close to equilibrium transition (sharp transition temperature);
(c) the temperature gradient in the standard during heating and cooling runs must be negligible, and
(d) the selected material must be stable at the temperature range used, i.e., it must not degrade.

Three successful liquid crystals were selected for the cooling calibration studies in [4–6]. These were *N*-(4-*n*-octyloxy-2-hydroxybenzal)-4′-*n*-butylaniline, and two liquid crystals from the Merck organization with trade names of CE-3 and CE-8 [7, 23–25] with the composition described below:

1. *N*-(4-*n*-octyloxy-2-hydroxybenzal)-4′-*n*-butylaniline (LC-1) (designated as LC-1 in [4–6]) prepared by Menczel and Leslie (Table 2)
2. (+)-4-*n*-hexyloxyphenyl-4′-(2″-methylbutyl)-biphenyl-4-carboxylate from the Merck organization with a commercial name of CE-3 (Table 3), and
3. (+)-(4-(2′-methylbutyl)phenyl-4′-*n*-octylbiphenyl-4-carboxylate), also from the Merck organization with a commercial name of CE-8 (Table 4)

It was noticed that the purity of the liquid crystals does have some effect on the Ch → I transition temperature hysteresis: if the purity falls below ∼99.4–99.7%, some supercooling can be observed during the cooling run (this

Table 2 The transitions in liquid crystal LC-1 [*N*-(4-*n*-octyloxy-2-hydroxybenzal)-4′-*n*-butylaniline]

Transition	T_t/°C*
Cr → S_C	39.2
S_C → N	69.4
N → I	89.2

* T_t is the transition temperature

Table 3 The transitions in liquid crystal CE-3 [(+)-4-*n*-hexyloxy-phenyl-4′-(2″-methylbutyl)-biphenyl-4-carboxylate]

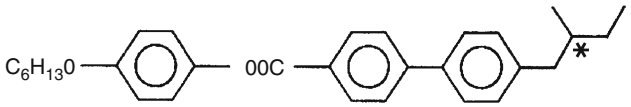

Transition	T_t/°C
Cr → S_C*	66.0
S_C* → Ch	78.8
Ch → I	163.5

Table 4 The transitions in liquid crystal CE-8 (+)-(4-(2′-methylbutyl-4′-octylbiphenyl-4-carboxylate)

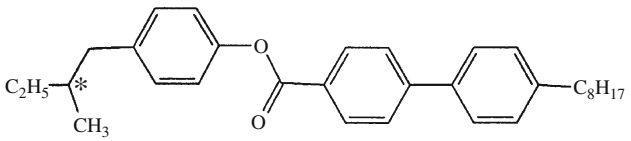

Transition	T_t/°C
Cr → S_J*	52.8
S_J* → S_I*	63.9
S_I* → S_C*	69.2
S_C* → S_A*	Not detectable by DSC (84.0 °C by microscopy)
S_A* → Ch	134.8
Ch → I	140.7

supercooling is usually <0.5 °C at ca. 99.0% purity). Therefore, in order to achieve an ∼0.1 °C accuracy, it is necessary to purify the standards to ca. 99.7–99.9%, and sometimes this may be difficult, as described in [5] for CE-8. The van't Hoff method can then be easily applied for the purity determination using the crystal → 1st liquid crystal transition as can be seen in Fig. 8a.

At the same time, it was noted that the DSC purity determination cannot be performed from any LC → LC or LC → I transition: when it was attempted to apply the van't Hoff equation to any LC → LC or N → I or Ch → I transitions, the calculation always gave 100% purity as illustrated in Fig. 8b.

The Ch → I or N → I transitions are very narrow, these transitions are very close to equilibrium transitions, so the extrapolated onset temperature must be used as the

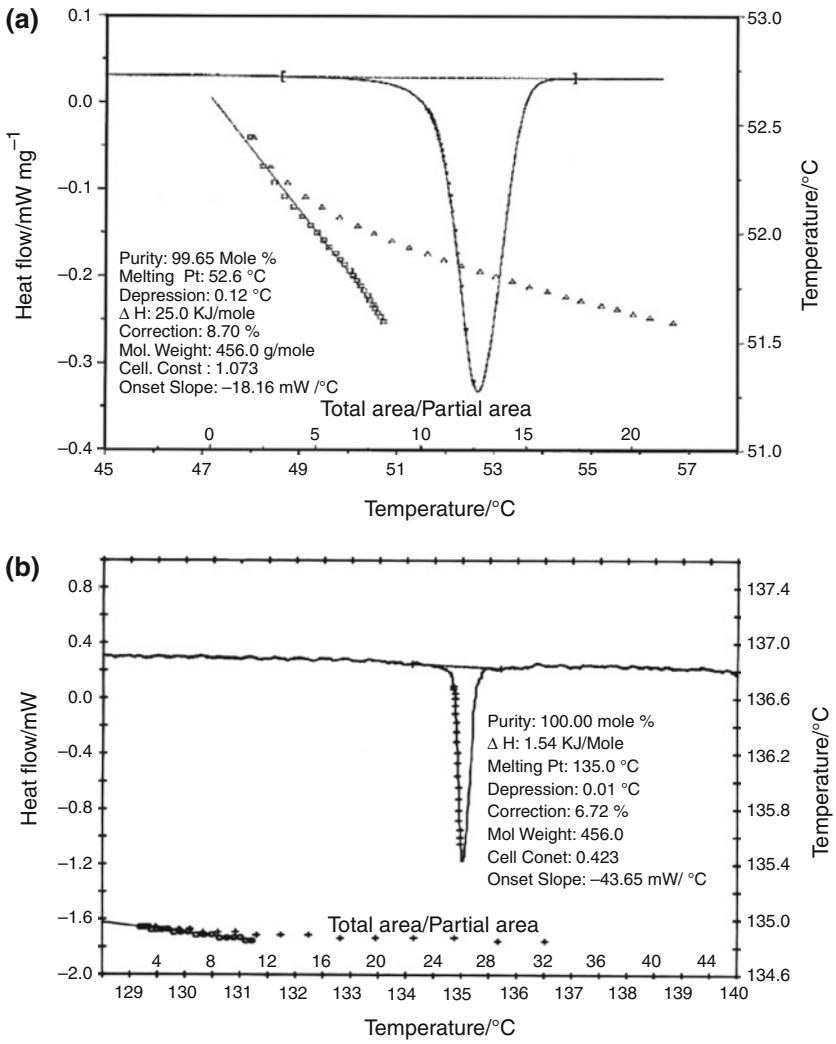

Fig. 8 DSC purity determination from the crystal → S_J* (**a**) and S_A* → Ch (**b**) transitions of liquid crystal CE-8. The purity from the crystal → S_J* transition is 99.65 mol%, while 100 mol% was obtained when the van't Hoff equation was applied to the S_A* → Ch transition. TAI 2920 DSC, endotherm is down

transition temperature. This was also supported by polarization optical microscopy observations.

The temperature gradient in the samples was calculated, and it was shown to be less than 0.1 °C for a heating or cooling rate of ≤80 °C/min, when the sample weight does not exceed 4 mg [4–6].

Another issue during the cooling calibration is the reproducibility of the transition temperature. The standards are (high purity) organic substances, and any considerable degradation will push down the transition temperatures and will likely cause hysteresis in the transition temperature. Of course, LC samples degraded to different degrees will give somewhat different transition temperatures. Therefore, the thermal stability of these standards must be thoroughly checked. This is best done by cyclic heating–cooling experiments, as shown in Fig. 9 for liquid crystal CE-8. In such series of experiments, a standard is heated, then cooled, and this is repeated several times, and the transition temperatures are calculated. As an example, the transition temperatures for smectic C → nematic and nematic → isotropic transitions for *N*-(4-*n*-octyloxy-2-hydroxybenzal)-4′-*n*-butylaniline (LC-1) recorded during cyclic heating and cooling are summarized in Table 5 for heating and cooling rates of 2 °C/min. In Table 5, T1 is the smectic C → nematic transition temperature, while T2 is the nematic → isotropic transition temperature. These transition temperatures do exhibit some minor decrease in the subsequent cycles due to some minor degradation, but this decrease is small (not more than 0.03–0.04 °C), essentially smaller than the accuracy of the cooling calibration. Therefore, for this liquid crystal, the effect of any degradation on the transition temperature can be neglected. Similar results were obtained for liquid crystals CE-3 and CE-8.

Finally, an important condition is that the environmental temperature in the laboratory must be constant (it should be kept within ±1 °C).

After these preliminary precautions (minimizing the temperature gradient in the standard, ensuring the

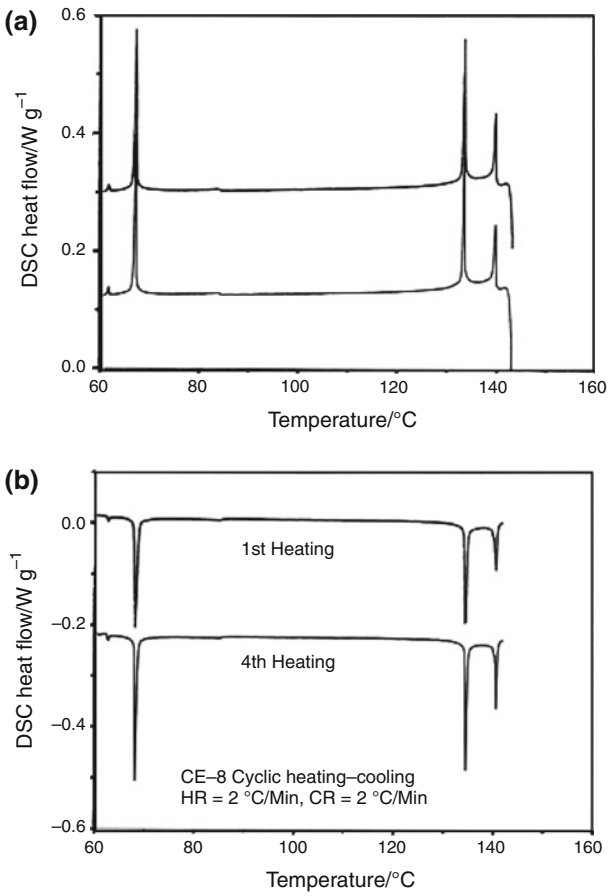

Fig. 9 Cooling (**a**) and heating (**b**) curves recorded on liquid crystal CE-8 heated-and-cooled cyclically on the same sample. The 1st and 4th coolings (**a**) and 1st and 4th heating curves (**b**). TAI 2920, cooling-and-heating rates = 2 °C/min, endotherm is down

necessary purity and preventing any considerable degradation), the cooling calibration can be performed.

Originally the cooling calibration was carried out using the N → I and the Ch → I transition temperatures (clearing point). The course of the cooling calibration was as follows:

a. Calibrate the instrument on heating at a definite heating rate to ±0.1 °C using high purity metals (In, Pb, Zn) and high (spectroscopic) purity water.
b. Load the standard into the cell, raise the temperature into the isotropic phase in order to ensure that a thin film is formed on the bottom of the sample pan, and cool it back into the crystalline state.
c. Reheat the standard and measure the clearing point on the second heating. In all the calculations, the clearing point on heating must be taken from the second heating experiments, since in this case the standard forms a thin film layer in the sample pan, so the thermal contact is better than in the first heating.

Table 5 The transition temperatures [smectic C → nematic (T_1) and nematic → isotropic (T_2)] on *N*-(4-*n*-octyloxy-2-hydroxybenzal)-4′-*n*-butylaniline recorded during cyclic heating and cooling

	T_1*/°C	T_2*/°C	ΔT_1/°C	ΔT_2/°C
Heating				
1st	69.44	89.20		
2nd	69.42	89.19		
3rd	69.41	89.18		
4th	69.40	89.17		
Cooling				
1st	69.15	88.95	0.29	0.25
2nd	69.14	88.95	0.28	0.24
3rd	69.13	88.95	0.28	0.23
4th	69.12	88.94	0.28	0.23
Average			0.28±0.01	0.24±0.01
			0.26±0.03	

ΔT_1 and ΔT_2 indicate the nominal temperature difference between the transition temperatures measured on heating and on cooling. Heating rate = 2 °C/min, cooling rate = 2 °C/min

* These data also indicate that the temperature reproducibility of the TAI 2920 was at least ±0.01 °C

After these experiments, the cooling calibration can be characterized as follows:

$$T_{\text{real}} = T_{\text{ind}} + \Delta T \tag{5}$$

or

$$T_{\text{clearing}} = T_{\text{itn}} + \Delta T \tag{6}$$

where T_{real} and T_{clearing} is the clearing point measured on heating, T_{ind} (T indicated) and T_{itn} (T isotropic-to-nematic) is clearing point measured on cooling at a desired cooling rate. Thus, ΔT can be calculated for all the necessary combinations of the heating and cooling rates, and used to determine the exact temperature during the cooling experiments.

The ΔT results calculated from the N → I and the Ch → I transitions were compared with the results obtained for several LC → LC transitions, and identical values were obtained. An example of this is shown in Table 5. This observation is very important, and it means that the supercooling is absent not only for the N → I and the Ch → I transitions, but for all the transitions involving a liquid crystalline phase (with the exception of the transitions involving the transition to the three-dimensional crystal). And this is not surprising, because similar to the nematic or cholesteric nuclei present in the isotropic liquid, the nuclei of other liquid crystalline phases must also be present in the next higher temperature liquid crystalline phase due to high molecular mobility and density fluctuations. Similar results were obtained for liquid crystals CE-3 and CE-8. Thus, it is advantageous to use liquid crystal

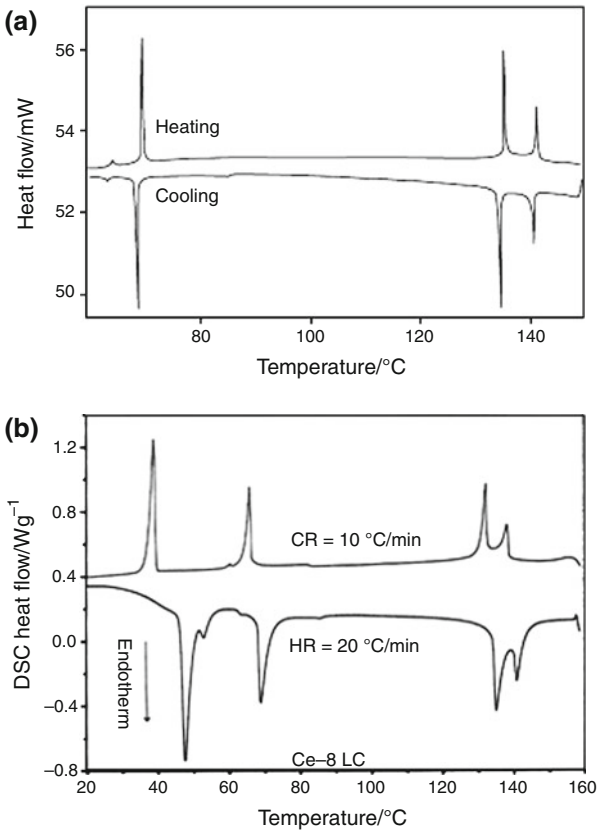

Fig. 10 The heating and cooling curves recorded on a CE-8 liquid crystal sample using TAI 2920 DSC. (**a**) Heating rate = 2 °C/min, cooling rate = 2 °C/min. (**b**) Heating rate = 10 °C/min, cooling rate = 20 °C/min. Endotherm is down

standards having several liquid crystalline phases: in such a case, all the transition temperatures can be used for the cooling calibration and the accuracy of the calibration can be improved.

Figure 10 shows the DSC curves of liquid crystal CE-8 on heating and cooling at considerably different heating and cooling rates measured on a TAI 2920 DSC. As expected, at low heating and cooling rates, the transitions are narrow and they become considerably broader at higher rates.

The results of the cooling calibration for a TAI 2920 DSC and Perkin-Elmer DSC7 are shown in Table 6 (the numbers before the slash indicate ΔT from Eq. 2 for a TAI 2920, while those after the slash represent the data for a Perkin-Elmer DSC7). The data indicate that ΔT for both instruments is very small for low heating and cooling rates, but it increases with increasing heating and/or cooling rates. Its value can reach 6–7 °C when the instrument is calibrated at 80 °C/min heating rate, and then run at a rate of cooling of 80 °C/min. This large ΔT value needs to be taken into account for polymer crystallization studies, because modeling processing conditions requires high cooling rates [26]. At cooling rates of not higher than 10 °C/min, the indicated temperature does not deviate more than 1 °C from the real temperature.

The experiments carried out with the liquid crystal standards at various cooling rates confirmed that neither the N → I (and the Ch → I) transition nor the LC → LC transitions have supercooling at cooling rates, of at least up to 160 °C/min (this was the highest cooling rate used with a Perkin-Elmer DSC7 calibration). Thus, it is possible that these transitions are cooling rate independent at higher ramp rates, as well, and this may explain why in liquid crystal materials the isotropic melt cannot be quenched even at extremely high cooling rates.

Unfortunately, the CE-3 and CE-8 liquid crystals are not available any longer commercially. The cooling calibration results described above were the basis in developing the ASTM 2069-06 standard [27]. This ASTM standard uses three other commercially available liquid crystals with the following transition temperatures:

- M24 (4-cyano-4′-octyloxybiphenyl): $S_A \rightarrow N$ at 67.1 °C, N → I at 79.8 °C
- HP-53 [4-(4-pentyl-cyclohexyl)-benzoic acid-4-propyl-phenyl ester: $S_A \rightarrow N$ at 92.9 °C, N → I at 120.4 °C

Table 6 Temperature calibration data on cooling calibration using a TAI 2920 DSC and Perkin-Elmer DSC7

	ΔT*				
Cooling rate/°C min^{-1}	1	2	5	10	20
Heating rate/°C min^{-1}					
2	0.2/−0.4	0.23/−0.2	0.37/−0.1	0.64/0.1	1.08/0.4
5	0.37/−0.2	0.37/0.1	0.55/0.3	0.67/0.5	1.07/0.9
10	0.55/0.0	0.76/0.3	0.75/0.5	0.78/0.7	1.28/1.3
20	0.90/0.6	0.95/0.7	1.07/0.9	1.41/1.2	1.68/1.7
40	1.66/1.1	1.86/1.3	1.83/1.4	2.20/1.6	2.3/2.1

* $\Delta T = T_{real} - T_{ind}$. The numbers before the slash indicate ΔT for a TAI 2920, while those after the slash represent the data for a Perkin-Elmer DSC7

– BCH-52 [4′-ethyl-4-(4-propyl-cyclohexyl)-biphenyl]: $S_B \rightarrow N$ at 92.9 °C

Thus, the results reported here were later used for shifting the cooling DSC curves, when the glass transitions recorded during heating and cooling had to be overlaid.

The absence of the hysteresis peak at the glass transition of semicrystalline polymers—slow cooling, fast reheating

Amorphous polymers

It is well known that the glass transition is a kinetic transition, therefore, it must have some time dependence. This can be illustrated by recording the glass transition of amorphous PET on cooling at various rates (see Fig. 11): when the cooling rate of amorphous PET decreases from 20 to 5 °C/min, and then to 1 °C/min, the glass transition temperature measured on cooling, visibly decreases. One of the consequences of the time dependence of the glass transition temperature is the appearance of the so-called hysteresis peak at the glass transition: when an amorphous polymer is cooled below T_g, and then re-heated at a higher rate, an endothermic hysteresis peak appears at the higher temperature side of the glass transition (see Figs. 12, 13). At a given heating rate, the intensity of the hysteresis peak increases with decreasing cooling rate.

Wunderlich was the first to give an explanation for the origin of the hysteresis peak (see, e.g., [28]): since the glass transition is a kinetic transition, the glass transition temperature is a function of the cooling and heating rate. Therefore, if we cool a polymeric melt that is unable to crystallize, the glass transition temperature on cooling will be lower than the glass transition temperature measured on subsequent re-heating if the heating rate is higher than the preceding cooling rate (Fig. 14). In a DSC experiment, the area under the full curve (provided that the recording started at 0 K) is proportional to the absolute enthalpy:

$$H_{0\rightarrow T} = \int_0^T C_p \mathrm{d}T \tag{7}$$

And since the absolute enthalpy of the sample in the melt at any temperature must have one definite value, the area difference between the cooling and heating curves must be compensated by another area that will have the appearance of the hysteresis peak. According to the 1st law of thermodynamics, the two shaded areas in Fig. 14 must be equal, i.e.

$$\Delta H_1 = \Delta H_2. \tag{8}$$

Figure 15 shows the experimental DSC curves for polystyrene (the cooling and heating rates were 2 and

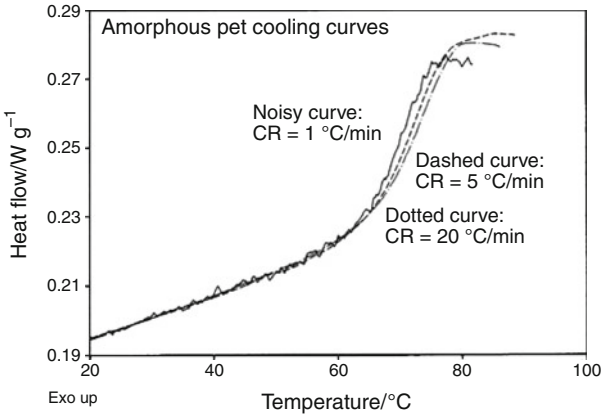

Fig. 11 Cooling curves of amorphous PET in the glass transition region. Cooling rates: 1 °C/min (*noisy curve*), 5 °C/min (*dashed curve*), and 20 °C/min (*dotted curve*) (TAI Q200, endotherm is down)

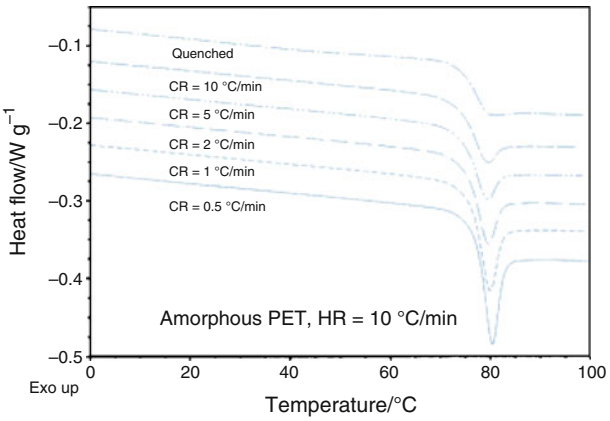

Fig. 12 The glass transition curves of amorphous PET recorded on heating at a rate of 10 °C/min on samples prepared by cooling at various rates. The cooling rate is indicated at each curve. Q200 TAI DSC, endotherm is down

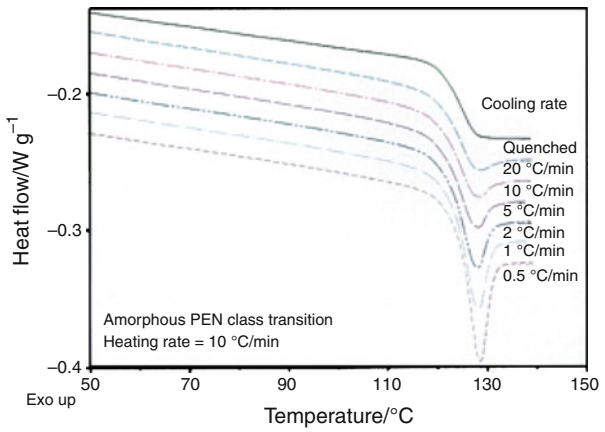

Fig. 13 The glass transition curves of amorphous PEN recorded on heating at a rate of 10 °C/min on samples prepared by cooling at various rates. The cooling rate is indicated at each curve. Q200 TAI DSC, endotherm is down

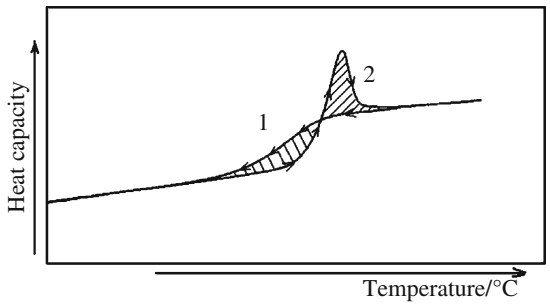

Fig. 14 A schematic figure explaining the origin of the hysteresis peak at the glass transition when the cooling rate is smaller than the rate of subsequent heating

10 °C/min, respectively). It also needs to be mentioned that a similar endothermic hysteresis peak is recorded when the glassy polymer is annealed below T_g. However, this relaxation behavior must be principally different from the slow cooling-fast reheating case, because, as will be seen later, the annealing hysteresis peak can be created for semicrystalline polymers, but the slow cooling-fast reheating hysteresis peak has never been observed for them.

Also, when the cooling rate is considerably higher than the subsequent heating rate, an exothermic hysteresis peak appears on the low temperature side of the glass transition, but this time this hysteresis peak is very shallow and broad. Finally, when the heating and cooling rates are equal (Fig. 16), an endothermic hysteresis peak is recorded similar to the case of slow cooling-fast reheating. Some researchers speculated that this hysteresis peak appears because the polymer is annealed during the heat-up. This explanation may not be correct, because in the case of

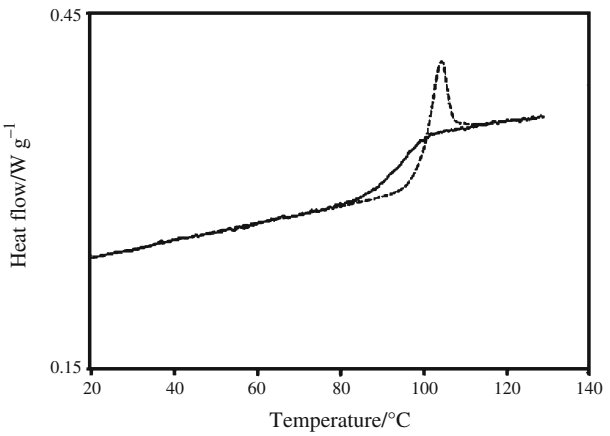

Fig. 15 The glass transition of polystyrene recorded on cooling (*solid line*, cooling rate = 2 °C/min) and on reheating the same sample (*broken line*, heating rate = 10 °C/min). The two areas encompassed by the curves are equal. Endotherm is up. The ordinate is proportional to the heat capacity

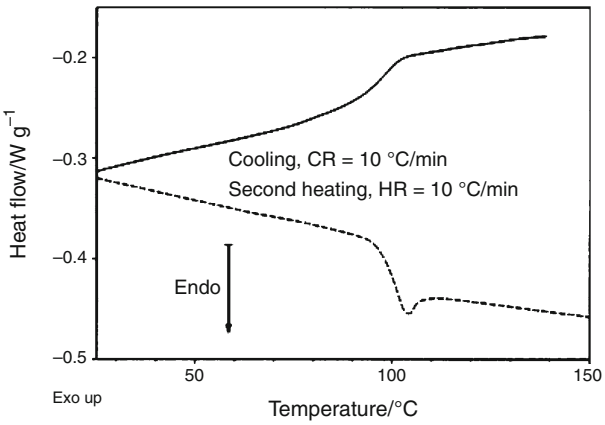

Fig. 16 The glass transition curves of PS recorded on cooling and reheating at equal rates (10 °C/min). The hysteresis peak on the heating curve is clearly visible, but this hysteresis peak cannot be observed for semicrystalline polymers. Q200 TAI DSC, endotherm is down

semicrystalline polymers such a hysteresis peak cannot be observed, although, as mentioned above, an annealing-related hysteresis peak *can* be induced for these samples.

Semicrystalline polymers

As mentioned before, in 1980 when the work on the glass transition of semicrystalline polymers was started [1], the available commercial instrumentation was not good enough to record the glass transition of amorphous or semicrystalline polymers on cooling. The baseline on cooling was not reproducible, and the temperature control in cooling experiments was often lost due to insufficient cooling capacity. And of course, the temperature calibration on cooling was not available. After the cooling calibration for DSC's was developed, and instruments like the Q-series DSC's of TAI cooled with an FTS mechanical cooling accessory were marketed (instruments with reproducible baselines on both heating and cooling), the glass transition curves from cooling and heating experiments could be compared.

Figure 17 shows a series of DSC curves of different crystallinity PET samples in the glass transition region at a heating rate of 10 °C/min after cooling all the samples at 1 °C/min. Similar to Fig. 2 of [1], the intensity of the hysteresis peak decreases with increasing crystallinity (the samples of various crystallinities were prepared by crystallizing PET at different cooling rates from the melt; then the samples were heated to 105 °C, and cooled at 1 °C/min. Finally, these samples were heated for analysis at a rate of 10 °C/min). It is obvious that that the developing crystals immobilize the amorphous regions, and the time dependence of the glass transition decreases with increasing crystallinity. Figure 18 shows the area under the hysteresis

peak as a function of crystallinity. As can be seen, the hysteresis peak disappears at ca. 29% crystallinity, so the question comes up whether the glass transition at this and higher crystallinities becomes time independent. If the glass transition is time independent then we should be able to superimpose the DSC curves on each other recorded on heating and cooling at various rates. Of course, the cooling curves first must be shifted according to the cooling calibration.

First, the reproducibility of the glass transition curves must be checked on a given instrument. Figure 19 shows the cooling DSC curves of a high crystallinity PET sample in two subsequent coolings: the curves are fully superimposable and the reproducibility of the Q200 DSC on cooling is excellent. Then, in two subsequent series of experiments, the following DSC curves were recorded:

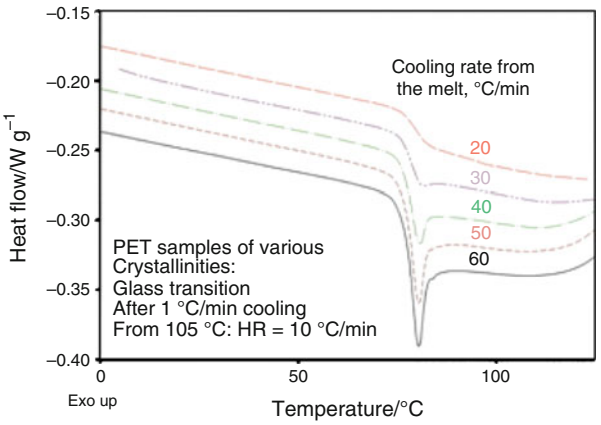

Fig. 17 The heating DSC curves of PET samples of various crystallinities (endotherm is down). The samples were prepared by cooling PET from the melt at various rates (the cooling rate is indicated at each curve). Then these samples were heated to 120 °C, cooled at 1 °C/min, and reheated again. These last reheating curves are shown in this figure (endotherm is down). The samples with the lowest cooling rates have the highest crystallinities. The intensity of the hysteresis peak decreases with increasing crystallinity. Q200 TAI DSC, endotherm is down

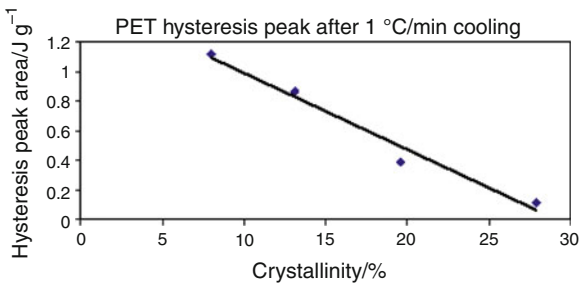

Fig. 18 The area under the hysteresis curve for semicrystalline PET samples cooled at 1 °C/min and reheated at 10 °C/min (the areas were calculated on curves shown in Fig. 11)

1. the cooling DSC curves in the glass transition region at various cooling rates
2. the heating and cooling DSC curves recorded at various rates

Finally, the obtained DSC curves were overlaid on each other.

Figures 20, 21, and 22 show the DSC curves recorded at 1 and 10 °C/min cooling for high crystallinity PET, Nylon 6, and PBT. Such a difference in the cooling rates produces marked differences in T_g of amorphous polymers, but the

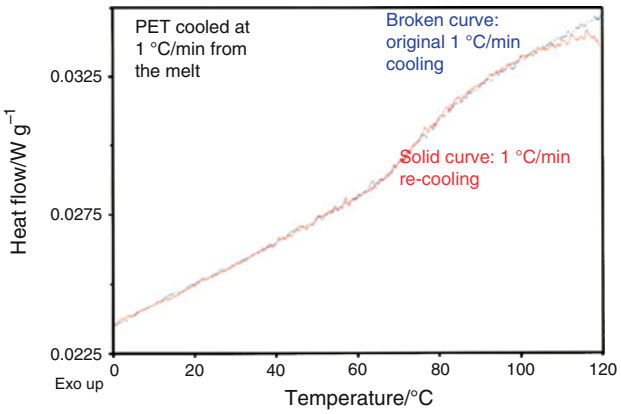

Fig. 19 Cooling DSC curves of semicrystalline PET in the glass transition region, for evaluating reproducibility of the DSC curves on cooling. The sample was crystallized at a rate of 1 °C/min, while cooling from 290 °C, cooled down to −80 °C ("top" curve), heated to 120 °C at 10 °C/min, cooled again at 1 °C/min (the curve with some deviation of the linearity of the heat capacity at 110–120 °C due to the program start). The two curves are superimposable (TAI Q200, endotherm is down)

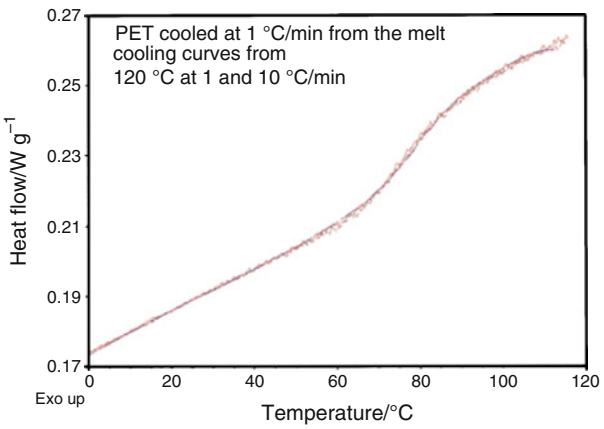

Fig. 20 Cooling curves of PET. Cooling rates of 1 and 10 °C/min on two different samples. Sample preparation: cooling at 1 °C/min from 290 °C, then heating to 120 °C. Curve (a) cooling at 1 °C/min; curve (b) cooling at 10 °C/min. TAI Q200 DSC. The two curves are superimposable (TAI Q200, endotherm is down)

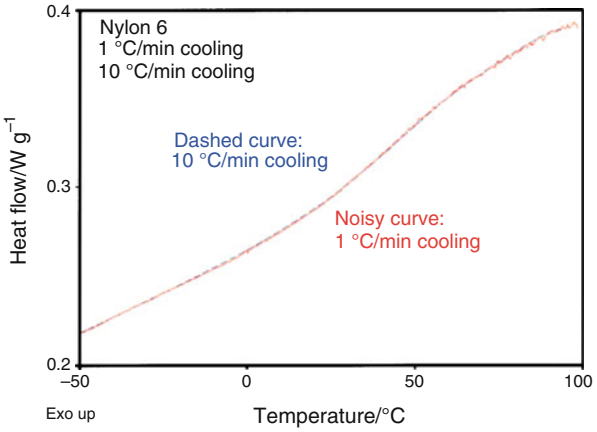

Fig. 21 Cooling curves of Nylon 6. Cooling rates of 1 and 10 °C/min on two different samples. Sample preparation: cooling at 1 °C/min from the melt, then heating to 100 °C. Curve (a) cooling at 1 °C/min; curve (b) cooling at 10 °C/min. TAI Q200 DSC. The two curves are superimposable (TAI Q200, endotherm is down)

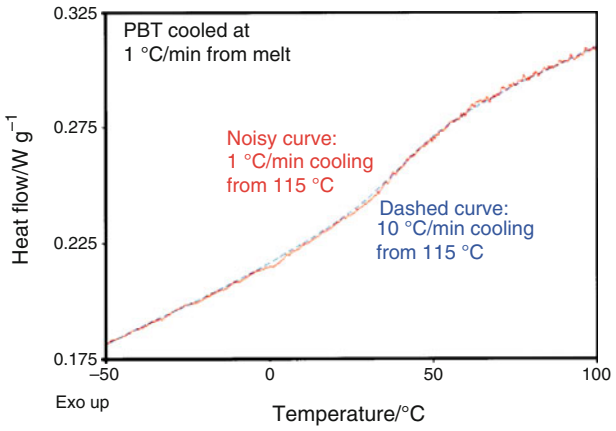

Fig. 22 Cooling curves of poly(butylene terephthalate). Cooling rates of 1 and 10 °C/min on two different samples. Sample preparation: cooling at 1 °C/min from 245 °C, then heating to 110 °C. Curve (a) cooling at 1 °C/min; curve (b) cooling at 10 °C/min. The two curves are superimposable (TAI Q200, endotherm is down)

curves of semicrystalline polymers are fully superimposable, at least they are very similar.

When the heating and cooling DSC curves recorded at 1 °C/min cooling and 10 °C/min heating are overlaid (Figs. 23, 24, 25, 26 for semicrystalline PET, polypropylene, PBT, and Nylon 6), definite differences were observed. The glass transition on heating is much narrower (remember, the ramp rate for heating is higher) than on cooling, but the midpoint of the glass transition is identical for both curves, and the areas encompassed by the two curves are identical. This shows some time dependence of the glass transition and it can also explain the absence of the hysteresis peak.

When we try to overlay the heating and cooling curves recorded at identical rates (i.e., +10 °C/min and −10 °C/min,

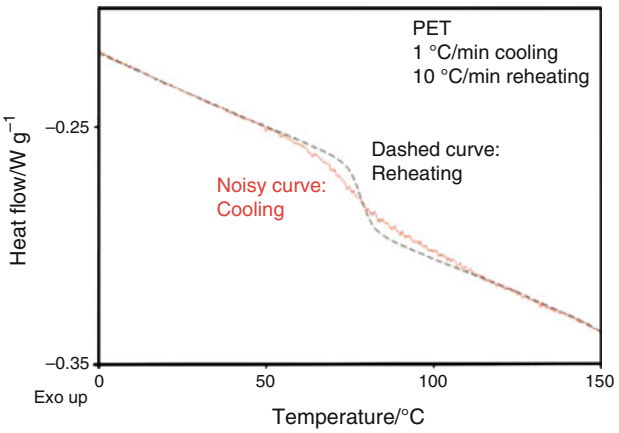

Fig. 23 Overlaying of heating and cooling curves of semicrystalline PET in the glass transition region on the same sample. Cooling rate 1 °C/min (*noisy curve*), then reheating at 10 °C/min (*dashed curve*). Sample preparation: cooling at 1 °C/min from 290 °C. TAI Q200 DSC. The two curves are not superimposable any more, although the midpoints are almost identical (TAI Q200, endotherm is down)

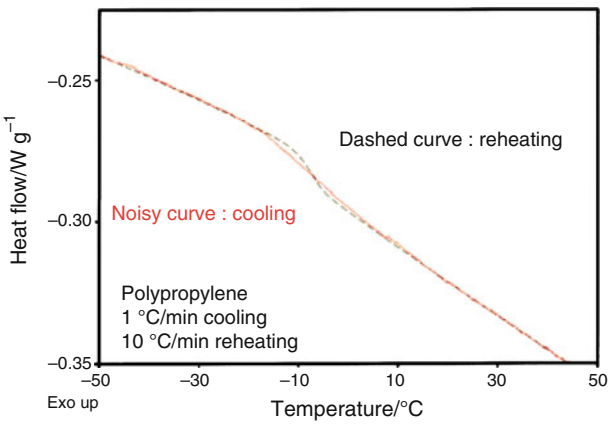

Fig. 24 Overlaying of heating and cooling curves of polypropylene in the glass transition region on the same sample. Cooling rate 1 °C/min (*noisy curve*), then reheating at 10 °C/min (*dashed curve*). Sample preparation: cooling at 1 °C/min from 220 °C. TAI Q200 DSC. The two curves are not superimposable, but the midpoint is almost identical like for other semicrystalline polymers (TAI Q200, endotherm is down)

see Fig. 27 for Nylon 6), the two curves are superimposable. Considering all these observations, we can state that the time dependence of the glass transition for semicrystalline polymers is drastically reduced, but is not totally gone. Also, it is clear that the width of the glass transition depends on the rate of heating or cooling, but it is the same for identical heating and cooling rates.

The results described here do contain some controversy. Repeating the above results

a. the glass transition curves recorded at CR = 1 and 10 °C/min cooling are identical (Figs. 20, 21, 22)
b. the glass transition recorded on cooling at CR = 1 °C/min is much broader than the glass transition recorded

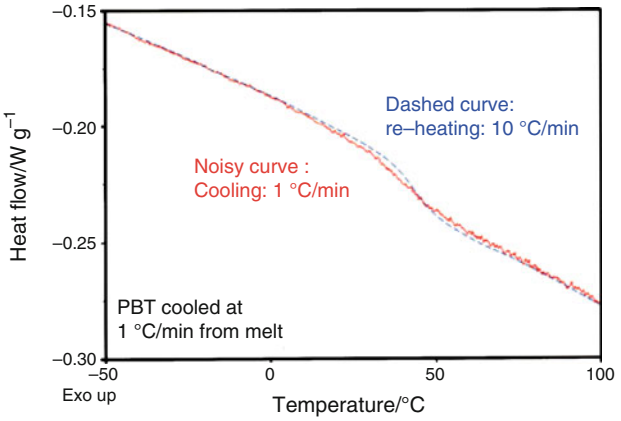

Fig. 25 Overlaying of heating and cooling curves of poly(butylene terephthalate) in the glass transition region on the same sample. Cooling rate 1 °C/min (*noisy curve*), then reheating at 10 °C/min (*dashed curve*). Sample preparation: cooling at 1 °C/min from 245 °C. TAI Q200 DSC. The two curves are not superimposable (endotherm is down)

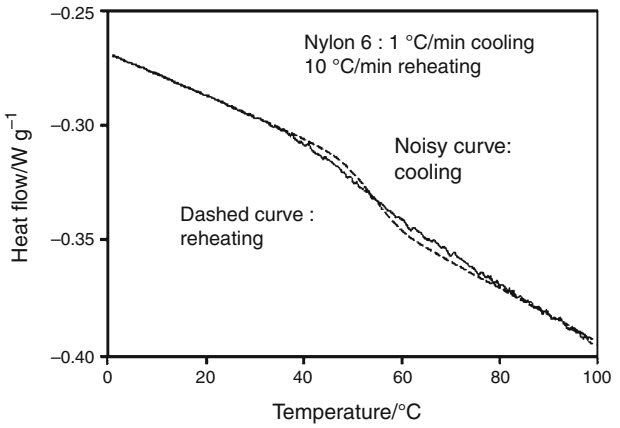

Fig. 26 Overlaying of heating and cooling curves of Nylon 6 in the glass transition region on the same sample. Cooling rate 1 °C/min (*noisy curve*), then reheating at 10 °C/min (*dashed curve*). Sample preparation: cooling at 1 °C/min from the melt. TAI Q200 DSC. The two curves are not superimposable, but the midpoints are similar (endotherm is down)

on a heating at HR = 10 °C/min (Figs. 23, 24, 25, 26), and

c. the glass transition curves recorded on cooling at CR = 10 °C/min and on heating at HR = 10 °C/min seem to be identical (Fig. 27).

Unfortunately, only one experiment has been made on the comparison of the glass transition curves recorded on both cooling and heating at 10 °C/min. It is necessary to check this result, but if it holds up, this would mean that the cooling of semicrystalline glasses at 1 and 10 °C/min produces glasses of different structures despite of the identical cooling curves.

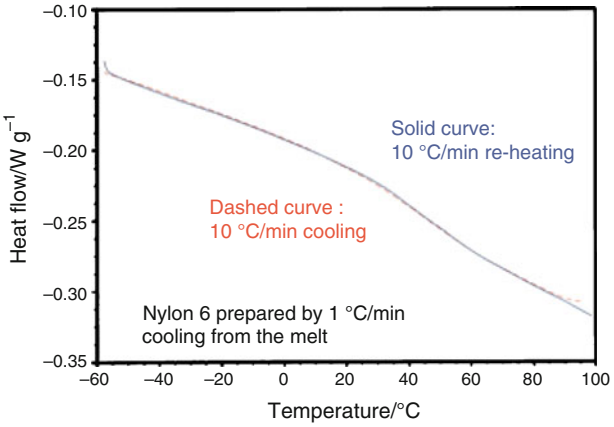

Fig. 27 Overlaying of heating and cooling curves of Nylon 6 in the glass transition region on the same sample. Cooling rate 10 °C/min (dashed curve), then reheating at 10 °C/min (*solid curve*). Sample preparation: cooling at 1 °C/min from the melt. TAI Q200 DSC. The two curves are superimposable (endotherm is down)

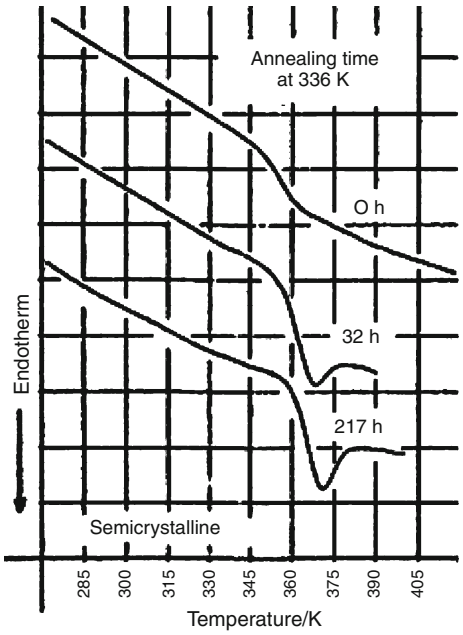

Fig. 28 The effect of the sub-T_g annealing on the glass transition of semicrystalline samples (PET): an endothermic hysteresis peak appears beyond the glass transition. Simultaneously, the glass transition is preceded by a broad sub-T_g exothermic peak. DuPont 990/910 DSC, endotherm is down. Reproduced from [1]

The hysteresis peak at the glass transition of semicrystalline polymers—case of sub-T_g annealing

Figures 28 [1] and 29 show the DSC curves of semicrystalline PET and PEN prepared by crystallization from the melt at slow cooling (1 °C/min in both cases) and annealing the samples for various times.

It is obvious that in the glass transition region, the annealing–cooling–reheating process leads to different

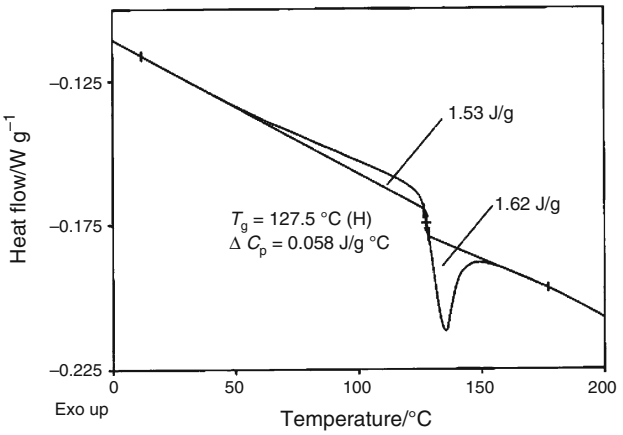

Fig. 29 The effect of the sub-T_g annealing on the glass transition of semicrystalline PEN. The sample was cooled at 1 °C/min from the melt and annealed 12.7 days at 102 °C. An endothermic hysteresis peak appears beyond the glass transition. Similar to PET (Fig. 28), in addition to the endothermic hysteresis peak, the glass transition is preceded by an extremely broad sub-T_g exothermic peak. The areas under the two peaks are similar. The accuracy of measuring the magnitude of the exothermic peak is low due to the extreme width of the peak. T_g is shifted upward when compared to non-annealed samples (TAI Q200, endotherm is down)

heating DSC curves than the slow cooling–reheating process. While for semicrystalline polymers, the latter does not produce any hysteresis peaks, two hysteresis peaks (a pre-glass transition exotherm and a post-glass transition endotherm) appear as a result of sub-T_g annealing. It is difficult to make a judgment on the relative areas under the endothermic and exothermic peaks, likely owing to the extreme width of the exothermic peak. For PEN (Fig. 29), similar areas were obtained. In another series of experiments with PET, the area under the exothermic peak was considerably smaller than that under the endothermic peak (Fig. 30). To further complicate the matter, the relative areas under the exothermic and endothermic peaks may, and probably, do depend on the annealing temperature. Further experiments are necessary to find the answer for this question. Together with the increase of mid-point T_g, ΔC_p and the relative areas under the peaks may clarify the source of this phenomenon. However, it is interesting to note that in some experiments the simultaneous exothermic–endothermic hysteresis peaks were recorded for amorphous polymers as well. This work is in progress [29], and its results may explain the differences of the sources of the annealing–reheating and the slow cooling–reheating hysteresis behavior.

Okazaki and Wunderlich [14] found that the activation energy of the glass transition decreases from 328 to 153 kJ/mol when comparing amorphous and semicrystalline PET samples. The ~328-kJ/mol value was re-generated after annealing somewhat below T_g. This may explain partially the reduction of the time dependence of the glass transition,

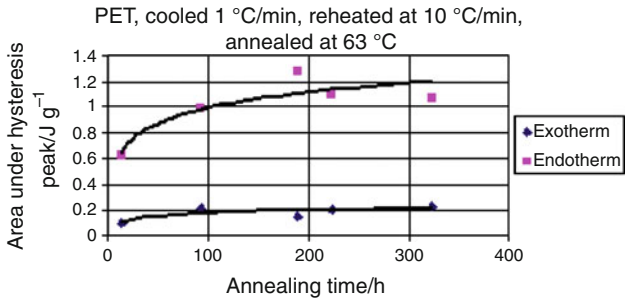

Fig. 30 The area under the exothermic and endothermic hysteresis peaks as a function of sub-T_g annealing time of semicrystalline PET. Annealing temperature 63 °C

but the question of the presence of the pre-transition exothermic hysteresis peak (i.e., some change in the kinetics of the glass transition) still remains open.

Some selected publications on the RAF

Below are listed some selected papers published on the amorphous phase in semicrystalline polymers:

- Ref. [1]: discovery of the ΔC_p deficiency and the missing hysteresis phenomenon (PET, Nylon 6, PEO, PCL, PVF, and Nylon 66)
- Ref. [10]: characterization of POM with heat capacity measurements
- Ref. [8]: characterization of the RAF in PC, PBT, and PET
- Ref. [30]: characterization of the RAF and the glass transition on heating and cooling in PET, PEN, PBT, Nylon 6, and PP
- Refs. [15, 16]: characterization of the RAF in PPS and PEEK by DEA
- Ref. [11]: characterization of the RAF in PET by MTDSC
- Ref. [31]: characterization of RAF in PPO
- Ref. [32]: characterization of RAF in PBT
- Refs. [19, 20]: study of the RAF in PE by TEM
- Refs. [21, 22]: study of the RAF in PE by solid state NMR
- Refs. [17, 18]: the crystal-amorphous interfacial layer in PE by density and heat of fusion measurements
- Ref. [9]: a summary paper on RAF in various semicrystalline polymers
- Ref. [33]: RAF in electrospun PET fiber
- Refs. [12–14]: MTDSC in biaxially oriented PET
- Ref. [13]: characterization of RAF by MTDSC in polycarbonate
- Refs. [34–36]: the amorphous phase in gel-spun PE fibers
- Ref. [37]: the RAF in poly(oxy-2,6-dimethyl-1,4-phenylene) (PPO)

Possible future work on the RAF

This work proved that the glass transition of semicrystalline polymers is a complex phenomenon. Since the RAF partially immobilizes the amorphous phase, its presence must change the properties of the polymers. Therefore, how can we use the RAF to achieve advantageous polymer properties? Here are several examples, in what direction research can proceed to use our knowledge about the RAF.

1. In the T_g–T_m region, the TAF is mobile, but RAF is still partially rigid. Therefore, with changing the content and the structure of the RAF, the mechanical properties of semicrystalline polymers will change. With a careful design of the RAF, we should be able to change the failure mechanism in semicrystalline polymers. The major source of ductility is segmental mobility, and if the mobility of the amorphous phase is obstructed by some barrier (which can be the RAF that, in addition to the interfacial layer, also contains the tie molecules), the internal crack formation and initiation of crack propagation may change. Toughness will definitely change. Therefore, the question comes up: will RAF make semicrystalline polymers more brittle above T_g compared to samples containing no RAF?
2. It is very important to clarify how we can prepare samples with different RAF content (and structure?):
   - Different crystallization conditions, e.g., comparing the three regimes of crystallization of Hoffman, must lead to different RAF structures
   - In certain semicrystalline polymers (PBT, see [9]) all the amorphous phase can be "rigid." It would be very important to clarify why this structure can exist in some polymers and whether we can induce similar structure in other polymers as well
   - The same content of the RAF in two samples does not mean identical structure of the RAF
3. The following techniques were used so far to characterize the RAF in semicrystalline polymers:
   - DSC (also MTDSC), DEA
   - Density measurements
   - Solid state NMR
   - WAXD
   - TEM

Conclusions

1. Semicrystalline polymers must be described by coexistence of the "mobile" or "traditional" amorphous phase, the crystal-amorphous transition layer ("rigid" amorphous fraction) and the crystalline phase.
2. Slow cooling followed by fast re-heating for semicrystalline polymeric samples does not induce an endothermic hysteresis peak. The absence of the hysteresis peak can be explained by a drastic decrease of the time dependence of the glass transition. However, some time dependence still can be observed. The DSC curves in the glass transition region recorded at different cooling and heating rates often are not superimposable, but the midpoint T_gs are almost identical.
3. The width of the glass transition of semicrystalline polymers is a complex issue, and the glass transition on heating may depend on the previous cooling rate
4. Annealing of semicrystalline samples does create an endothermic hysteresis peak, but with a simultaneous appearance of a broad pre-glass transition exothermic hysteresis peak indicating changes in the kinetics of the glass transition.
5. Modern DSC's can be calibrated to a high degree of accuracy using the N → I and Ch → I transitions (up to a CR of 160 °C/min). The accuracy of calibration is close to that on heating calibration with high purity metals (∼0.1 °C). Somewhat larger errors can be expected at cooling rates higher than 20 °C/min.
6. In addition to the nematic → isotropic and the cholesteric → isotropic transitions, LC → LC transitions do not have supercooling. Therefore, all the available LC → LC transitions can be used for temperature calibration (in the present work, the N → S_C, the Ch → S_C*, Ch → S_A, S_C* → S_I*, S_I* → S_J* transition were used)
7. In case of liquid crystalline substances, the van't Hoff equation of DSC purity determination is applicable only to the crystal → first liquid crystalline phase transition, but not to the LC → LC transitions, as well as to the N → I and Ch → I transitions.

References

1. Menczel J, Wunderlich B. J Polym Sci Polym Lett Ed. 1981;19:261.
2. Menczel J, Wunderlich B. J Polym Sci Polym Phys Ed. 1980;18:1433.
3. Meesiri W, Menczel J, Gaur U, Wunderlich B. J Polym Sci Polym Phys Ed. 1982;20:719.
4. Menczel J, Leslie T. Thermochim Acta. 1990;166:309.
5. Menczel J, Leslie T. J Therm Anal. 1993;40:957.
6. Menczel J, Leslie T. J Therm Anal. 1993;49:193.
7. EM Chemicals Technical Brochure EM-321S-84.
8. Menczel J, Wunderlich B. Polym Preprints (Div Polym Chem Am Chem Soc) 1986;27:255.
9. Wunderlich B. Prog Polym Sci. 2003;28:383.
10. Suzuki H, Grebowicz J, Wunderlich B. Br Polym J. 1985;17:1.
11. Chen H, Cebe P. Macromolecules. 2009;42:288.

12. Okazaki I, Wunderlich B. Macromolecules. 1997;30:1758.
13. Schick C, Wurm A, Mohammed A. Colloid Polym Sci. 2001; 279:800.
14. Okazaki I, Wunderlich B. J Polym Sci B. 1996;34:2941.
15. Pengtao H, Cebe P. J Polym Sci Polym Phys Ed. 1992;30:239.
16. Pengtao H, Cebe P. Macromolecules. 1992;25:902.
17. Mandelkern L, Alamo RG, Kennedy MA. Macromolecules. 1990; 23:4721.
18. Mandelkern L. Polym J. 1985;17:337.
19. Kunz M, Möller M, Heinrich U-R, Cantow H-J. Makromol Chem Symp. 1988;20/21:147.
20. Kunz M, Möller M, Heinrich U-R, Cantow H-J. Makromol Chem Symp. 1989;23:57.
21. Kitamaru R, Horii F, Murayama K. Macromolecules. 1989;23:57.
22. Cheng J, Fone M, Reddy VN, Schwartz KB, Fisher HP, Wunderlich B. J Polym Sci B. 1994;32:2683.
23. Gray GW, McDonnel DG. Mol Cryst Liq Cryst. 1976;37:189.
24. Gray GW, Goodby JW. Smectic liquid crystals, textures and structures. Glasgow, London: Leonard Hill; 1984. (and references therein).
25. Goodby JW, Gray GW. J Phys. 1979;40, Colloque C3, page C-3.
26. Lawton EL. Polym Eng Sci. 1985;25:348.
27. ASTM standard 2069-06. Test method for temperature calibration on cooling of differential scanning calorimeters.
28. Wunderlich B. Thermal analysis. Boston: Academic Press; 1998.
29. Menczel J (to be published).
30. Menczel J, Jaffe M. J Therm Anal Calorim. 2007;89:357.
31. Cheng SZD, Wunderlich B. Macromolecules. 1987;20:1630.
32. Cheng SZD, Pan R, Wunderlich B. Makromol Chem. 1988;189: 2443.
33. Chen H, Liu Z, Cebe P. Polymer. 2009;50:872.
34. Fu Y, Annis B, Boller A, Jin Y, Wunderlich B. J Polym Sci B. 1994;32:2289.
35. Fu Y, Busing WR, Jin Y, Affholter KA, Wunderlich B. Macromolecules. 1993;26:2187.
36. Kwon YK, Boller A, Pyda M, Wunderlich B. Polymer. 2000; 41:6237.
37. Pak J, Pyda M, Wunderlich B. Macromolecules. 2003;36:495.
38. Jackson WJ, Kuhfuss HF. J Polym Sci Polym Chem Ed. 1976;14: 2043.